

Multibranch gold nanoparticles coated with serum proteins fit for photothermal tumor ablation

EP SCI

Cite as: AIP Advances 10, 125030 (2020); <https://doi.org/10.1063/5.0025368>

Submitted: 17 August 2020 . Accepted: 29 November 2020 . Published Online: 30 December 2020

Clara Carreón-Álvarez,  José Luis Sánchez-García, Víctor Sanabria-Ayala, Luis Antonio Ortiz-Frade, Mario E. García-Rodríguez,  José Luis Rodríguez-López, and  Rubén López-Revilla

COLLECTIONS

Paper published as part of the special topic on [Chemical Physics](#), [Energy](#), [Fluids and Plasmas](#), [Materials Science](#) and [Mathematical Physics](#)

 This paper was selected as an Editor's Pick



View Online



Export Citation



CrossMark

ARTICLES YOU MAY BE INTERESTED IN

[Spiky piñata-shaped gold nanoparticles optimized for cancer treatments](#)

Scilight 2021, 011105 (2021); <https://doi.org/10.1063/10.0003269>

[Fluid dynamics simulations show that facial masks can suppress the spread of COVID-19 in indoor environments](#)

AIP Advances 10, 125109 (2020); <https://doi.org/10.1063/5.0035414>

[Curved-boundary particle-in-cell simulation for the investigation of the target erosion effect of DC magnetron sputtering system](#)

AIP Advances 10, 125224 (2020); <https://doi.org/10.1063/5.0035172>

AIP Advances
Fluids and Plasmas Collection

READ NOW

Multibranching gold nanoparticles coated with serum proteins fit for photothermal tumor ablation



Cite as: AIP Advances 10, 125030 (2020); doi: 10.1063/5.0025368
Submitted: 17 August 2020 • Accepted: 29 November 2020 •
Published Online: 30 December 2020



View Online



Export Citation



CrossMark

Clara Carreón-Álvarez,¹ José Luis Sánchez-García,²  Víctor Sanabria-Ayala,¹ Luis Antonio Ortiz-Frade,³ Mario E. García-Rodríguez,⁴ José Luis Rodríguez-López,^{5,a)}  and Rubén López-Revilla^{1,a)} 

AFFILIATIONS

¹División de Biología Molecular, Instituto Potosino de Investigación Científica y Tecnológica, Camino a La Presa San José 2055, 78216 San Luis Potosí, S.L.P., Mexico

²Facultad de Ciencias Químicas, Universidad Autónoma de San Luis Potosí, Av. Dr. Manuel Nava 6, 78210 San Luis Potosí, S.L.P., Mexico

³Centro de Investigación y Desarrollo Tecnológico en Electroquímica, Parque Tecnológico Querétaro s/n Sanfandila, 76703 Pedro Escobedo, Qro., Mexico

⁴Centro de Física Aplicada y Tecnología Avanzada, Universidad Nacional Autónoma de México, Blvd. Juriquilla 3001, 76230 Santiago de Querétaro, Qro., Mexico

⁵División de Materiales Avanzados, Instituto Potosino de Investigación Científica y Tecnológica, Camino a La Presa San José 2055, 78216 San Luis Potosí, S.L.P., Mexico

^{a)}Authors to whom correspondence should be addressed: jlrdez@ipicyt.edu.mx and rlopez@ipicyt.edu.mx

ABSTRACT

Photothermal tumor ablation might be carried out with multibranching gold nanoparticles (MBAuNPs) having maximum absorbance (A_{\max}) in the infrared region and functionalized with ligands that would bind them to the target tumor markers. However, in nanomedicine applications, the nanostructures must reach their target tissues to be effective, but the corona of serum proteins they instantaneously acquire when administered by intravenous injection may affect their activity; for this reason, we decided to analyze the effect that exposing MBAuNPs to bovine serum albumin (BSA) and human serum (HS) have on their protein corona and physical properties. The synthesized spherical Au seeds stoichiometrically generate *piñata*-like MBAuNPs of 8–20 peaks potentially useful for photothermal tumor ablation since they induce hyperthermia of more than 4 °C in phantom gels mimicking the skin irradiated with an 808 nm laser at 0.75 W/cm². The calculated surface area of MBAuNPs ranges from 24 984 nm² to 40 669 nm², depending on the number of peaks we use for modeling the NPs. When MBAuNPs are exposed to BSA, they acquire a protein corona with an internal “hard” portion composed by one or two layers of BSA containing ~1000–4000 molecules covalently bound to their surface, and an external “soft” portion formed by agglomerated BSA molecules linked by non-covalent bonds. Functionalization with BSA decreases the tendency of MBAuNPs to agglomerate and increases their size dispersion. MBAuNPs and MBAuNPs–BSA exposed to HS bind HS albumin and other HS proteins ranging from 25 kDa to 180 kDa that increase their hydrodynamic diameter and decrease their stability. We conclude that MBAuNPs exposed to serum albumin and HS instantaneously acquire a hard and soft protein corona that may affect prior or subsequent functionalization aiming to direct them to specific cell or tissue targets.

© 2020 Author(s). All article content, except where otherwise noted, is licensed under a Creative Commons Attribution (CC BY) license (<http://creativecommons.org/licenses/by/4.0/>). <https://doi.org/10.1063/5.0025368>

INTRODUCTION

Malignant tumors are usually treated by surgical resection, chemotherapy, and radiotherapy.¹ Chemotherapy and radiotherapy are often ineffective and have undesirable side effects because they do not discriminate between healthy and cancerous cells.² Although hyperthermia for tumor ablation is an alternative to surgical resection,³ it is rarely used because the temperature in the target tissue is not homogeneous.⁴ Since radiation in the near-infrared region (NIR) penetrates deeply but is hardly absorbed by tissues,^{5–7} attempts have been made to develop tumor ablation procedures based on nanoparticles (NPs) that convert NIR radiation into heat.² Gold NPs (AuNPs) are non-toxic,⁸ and since spherical AuNPs absorb NIR waves much less efficiently, nowadays the use of multi-branched AuNPs (MBAuNPs)⁹ for hyperthermal phototherapy is being intensively explored.¹⁰

Depending on the tumor and its anatomical location, the potential efficacy of photothermal nanotherapy would depend on both the photothermal conversion efficiency² and the ability of NPs to reach and penetrate the desired tumor targets.¹¹ NPs are functionalized with ligands that direct them to specific cell receptors,¹² but when they enter the bloodstream they are instantly modified through their interaction with blood proteins attaching to their surface and forming a structure known as protein corona (PC).^{11,13} The PC is formed by the hard corona (HC) consisting of proteins

strongly associated with the NP surface, and by the soft corona (SC) that is an outer layer of weakly bound proteins.¹⁴ The PC is also complex and unique for each nanomaterial and changes the physicochemical properties of NPs, such as size, surface charge, and state of aggregation.¹⁵ These changes may interfere with the functionalities provided in biological microenvironments.^{16,17} The development of NPs suitable for *in vivo* photothermal therapy thus depends on controlling PC formation and structure and its effects on the physical and biological properties of NPs.^{18,19}

In this report, we describe the synthesis of MBAuNPs, their characterization, and the features of the hard and soft protein corona they acquire after being exposed to bovine serum albumin (BSA), to human serum (HS), or BSA followed by HS. The photothermal tumor ablation potential of our MBAuNPs is supported by their high photothermal conversion efficiency leading to a net temperature increase of $\sim 5^\circ\text{C}$ in phantom gels irradiated at low power ($<1\text{ W/cm}^2$) with an 808 nm near-infrared laser.

RESULTS

Size, shape, and concentration of nanoparticles

Auric seeds

Scanning electron microscope (SEM) images showed that seeds were spherical, with a hydrodynamic diameter (D_H) of 18 nm

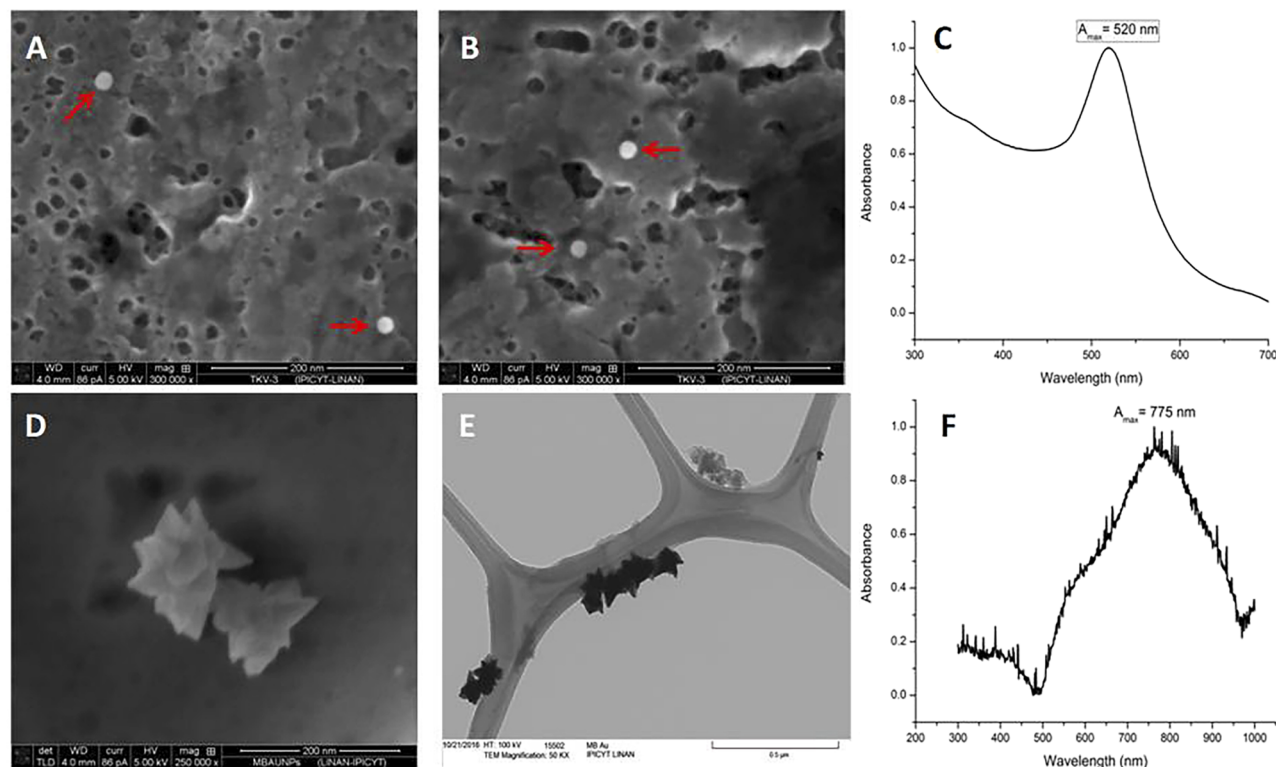


FIG. 1. Electron microscopy of auric seeds and MBAuNPs, and UV–VIS spectra of their suspensions. (a) and (b) Scanning electron microscope images of auric seeds (clear circles are indicated with red arrows), and (c) UV–VIS spectrum of their suspensions. MBAuNP images of scanning (d) and transmission (e) electron microscopy, and (f) UV–VIS spectrum of their suspensions. Both UV–VIS spectra were normalized to $A_{\max} = 1.0$.

TABLE I. Dynamic light scattering analyses of auric seeds, MBAuNPs, and MBAuNPs-BSA suspensions. ND: No determinate.

Sample	In PBS			In human serum		
	DH (nm)	PDI	ζ -potential (mV)	DH (nm)	PDI	ζ -potential (mV)
Seeds	18	0.602	-36.8	ND	ND	ND
MBAuNPs	125	0.455	-24.4	148	0.2048	-18
MBAuNPs-BSA	146	0.929	-72.7	185	0.1672	-31

[Figs. 1(a) and 1(b) and Table I], and a surface area of 1020 nm^2 , and maximum absorbance at 520 nm [Fig. 1(c)].

The ζ -potential of the seeds was -36.8 mV , with a polydispersity index (PDI) of 0.602 (Table I). The concentration determined by inductively coupled plasma atomic emission spectroscopy (ICP-OES) was 60 mg/l , corresponding to 1×10^{15} seeds/l.

MBAuNPs

SEM and transmission electron microscopy (TEM) images showed anisotropic multibranched nanoparticles with 8–20 peaks,

D_H of 125 nm [Figs. 1(d) and 1(e); Table I], maximum absorbance at 775 nm , and null absorbance at 520 nm [Fig. 1(f)]. The surface areas calculated for MBAuNPs containing 8, 12, and 20 peaks were 24984 nm^2 , 30212 nm^2 , and 40669 nm^2 , respectively.

The ζ -potential of MBAuNPs was -24.4 mV , with a PDI of 0.455 (Table I). The MBAuNP concentration determined by ICP-OES was 23.5 mg/l , corresponding to 1×10^{13} MBAuNPs/l.

Hyperthermia induced by irradiation of auric seeds and MBAuNPs in aqueous and phantom gel suspensions

The temperature was monitored in aqueous solutions containing auric seeds (60 mg/l), or MBAuNPs (23.5 mg/l), and in phantom

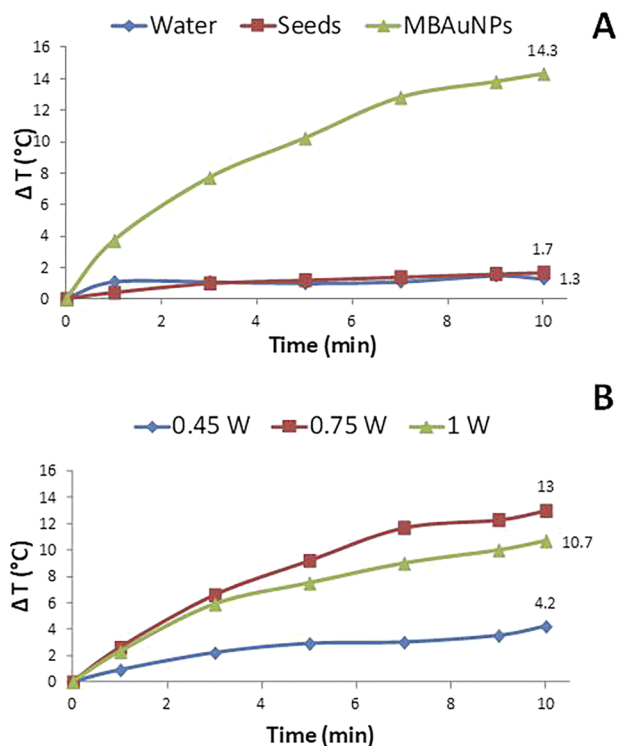


FIG. 2. Time course of the temperature in aqueous suspensions containing 100 times more auric seeds than MBAuNPs and irradiated with an 808 nm laser at increasing power. Suspensions containing 1×10^{12} seeds ($60 \mu\text{g}$)/ml or 1.5×10^{11} MBAuNPs ($23.5 \mu\text{g}$)/ml were irradiated continuously with different powers of an 808 nm laser. (a) MBAuNPs and seed suspensions irradiated with 0.75 W/cm^2 . (b) MBAuNP suspensions irradiated with 0.45 W/cm^2 , 0.75 W/cm^2 , or 1 W/cm^2 . Error of temperature measurements: $\pm 2\%$.

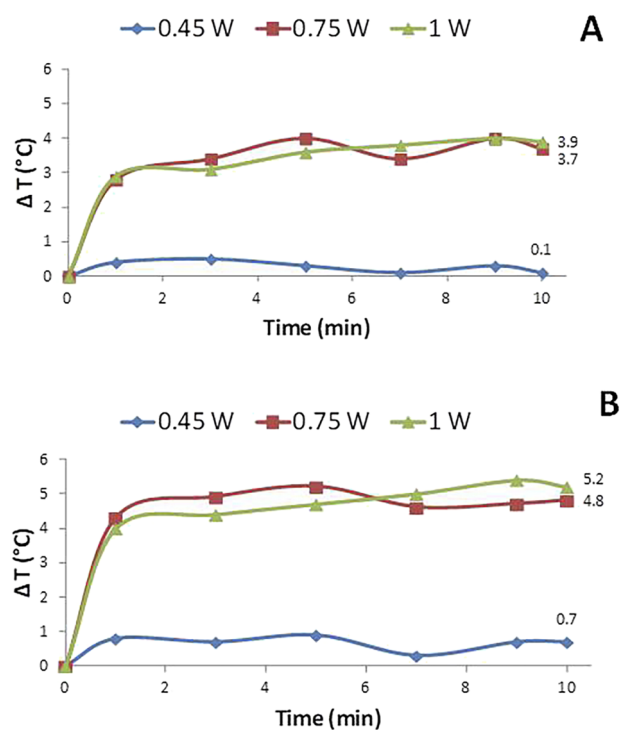


FIG. 3. Time course of the temperature in phantom gel suspensions containing different concentrations of MBAuNPs, irradiated with increasing powers of an 808 nm laser. (a) Phantom gel with 1.3×10^{10} MBAuNPs ($2 \mu\text{g}$) per ml. (b) Phantom gel with 1.9×10^{10} MBAuNPs ($3 \mu\text{g}$) per ml. Error of temperature measurements: $\pm 2\%$.

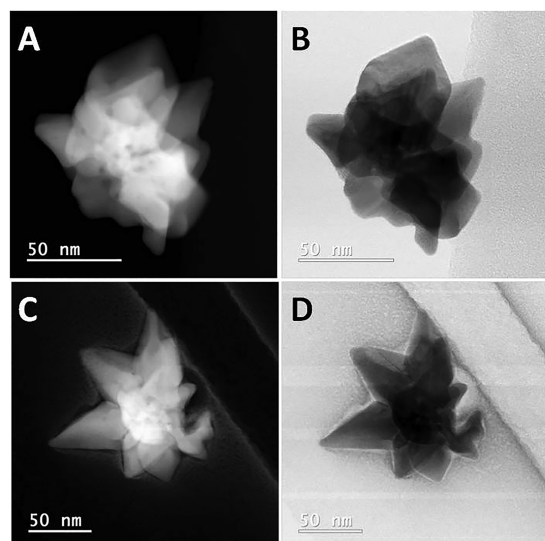


FIG. 4. Dark- and clear-field HRTEM images from MBAuNPs and MBAuNPs-BSA stained with uranyl acetate. MBAuNPs in dark field (a) and clear field (b). MBAuNPs-BSA in dark field (c) and clear field (d).

gels containing MBAuNPs (2 mg/l or 3 mg/l). All samples were irradiated continuously for 10 min with an 808 nm laser at irradiation powers of 1 W/cm², 0.75 W/cm², and 0.45 W/cm².

The increase of temperature in water and aqueous suspensions irradiated with fixed 0.75 W/cm² power was: water, 1.3 °C; auric seeds, 1.7 °C; MBAuNPs, 14.3 °C [Fig. 2(a)]. The increase of temperature in aqueous MBAuNP suspensions irradiated with increasing powers (subtracting the increase in water) was: 0.45 W/cm², 4.2 °C; 0.75 W/cm², 13 °C; 1 W/cm², 10.7 °C [Fig. 2(b)].

The increase of temperature in phantom gels containing MBAuNPs (2 mg/l) irradiated with increasing powers was: 0.45 W/cm², 0.1 °C; 0.75 W/cm², 3.7 °C; 1 W/cm², 3.9 °C [Fig. 3(a)]. The increase of temperature in phantom gels with MBAuNPs

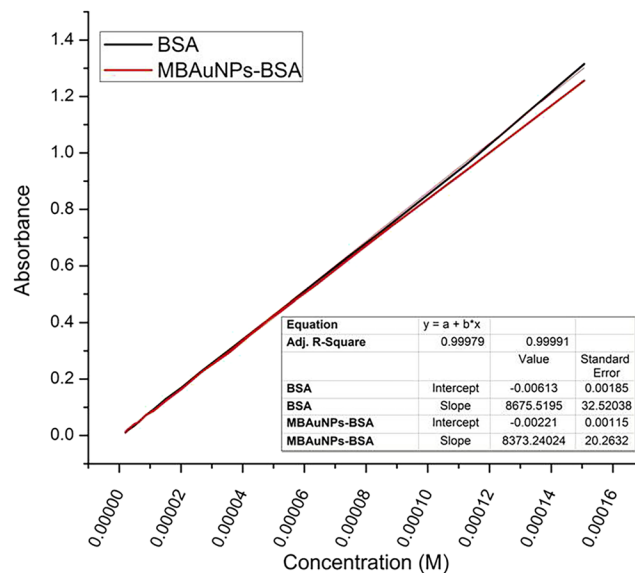


FIG. 6. Calibration curves of BSA in solution and MBAuNPs-BSA suspension. Concentrations of BSA in solution and MBAuNPs-BSA suspensions ranged from 0.13 mg/ml to 10 mg/ml (2 μM–1500 μM). Equivalent BSA concentrations were used for BSA in solution and MBAuNPs-BSA (7.6×10^{11}). Black line: BSA solution. Red line: MBAuNPs-BSA.

(3 mg/l of Au) irradiated with increasing powers was: 0.45 W/cm², 0.7 °C; 0.75 W/cm², 4.8 °C; 1 W/cm², 5.2 °C [Fig. 3(b)].

Surface area and BSA corona in MBAuNPs

TEM and high-resolution transmission electron microscope (HRTEM) images of functionalized MBAuNPs showed a 10 nm–15 nm thick layer covering their surface that was absent in pure MBAuNPs (Fig. 4). D_H values increased from 125 nm for MBAuNPs to 146 nm for MBAuNPs-BSA. The ζ-potential of MBAuNPs was –72.7 mV, with a PDI of 0.929 (Table I).

The UV–VIS spectra of pure BSA in solution and MBAuNP suspensions functionalized with BSA were determined using

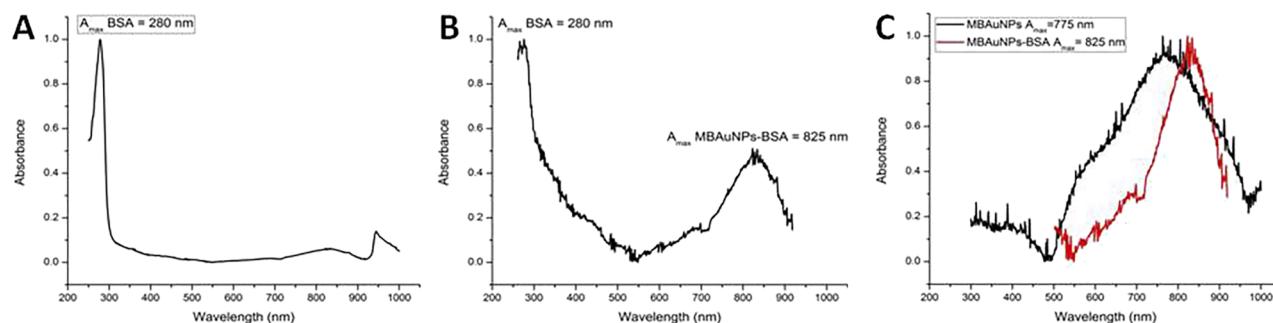


FIG. 5. UV–VIS spectra of BSA in solution, and MBAuNPs, and MBAuNPs-BSA suspensions. All samples contained 10 μg/μl BSA, whose maximum absorbance value (at 280 nm) was normalized as 1.0. (a) BSA solution. (b) MBAuNPs-BSA suspension. (c) Comparison of the 300 nm–1000 nm UV–VIS spectra from MBAuNPs (black line) and MBAuNPs-BSA (red line).

phosphate-buffered saline (PBS) as a vehicle. The absorbance peaks observed were as follows: pure BSA, a single peak at 280 nm; pure MBAuNPs, a single peak at 775 nm; MBAuNPs-BSA, two peaks, a major one at 280 nm and a minor one at 825 nm (Fig. 5).

The molar extinction coefficient of BSA in solution was $43\,377\text{M}^{-1}\text{cm}^{-1}$, and that of BSA bound to MBAuNPs was $41\,866\text{M}^{-1}\text{cm}^{-1}$ (Fig. 6).

The average number of BSA molecules in a suspension containing 7.6×10^{11} MBAuNPs/ml was calculated by UV spectroscopy. The BSA concentration in MBAuNP-BSA sedimented by centrifugation and resuspended in PBS was 4.5×10^{16} molecules/ml, corresponding to 59 210 BSA molecules per MBAuNP. MBAuNPs-BSA suspensions washed six times with PBS contained 1.14×10^{15} BSA molecules/ml, corresponding to 1500 BSA molecules per MBAuNP (2.5% of the total BSA molecules initially bound).

Through mathematical estimation of the surface area of MBAuNPs and taking into account the area of individual BSA molecules, we calculated 3.5×10^{12} molecules/cm², assuming that the hard protein corona formed by a molecular monolayer would amount to ~900, ~1000, and ~1500 BSA molecules per MBAuNP with 8, 12, and 20 tips, respectively. Assuming a protein bilayer, the number of BSA molecules per MBAuNP would be ~1900, ~2500, and ~3880 (Table II).

XPS spectra of MBAuNPs-BSA. The high-resolution x-ray photoelectron spectroscopy (XPS) spectrum of gold in pure MBAuNPs had three peaks (including their doublets) at 82.37 eV, 82.87 eV, and 85.06 eV, corresponding to Au⁰, Au¹⁺, and Au³⁺, respectively. In contrast, the high-resolution spectrum of gold in MBAuNPs-BSA had two peaks: the first at 81.31 eV identified as Au⁰ and the second at 82.11 eV identified as a C-S-Au (I) bond [Figs. 7(a) and 7(b) and Table III]. The high-resolution spectrum of sulfur had the main peak at 166.21 eV, corresponding to the S 2p_{3/2} position identified as an S-Au bond [Table III and Fig. 7(c)].

Circular dichroism of BSA in solution and MBAuNPs-BSA

BSA in solution and MBAuNPs-BSA suspensions had the 208 nm and 222 nm absorbance peaks characteristic of α -helix structures. The α -helix contents of solutions with 0.25 mg/ml, 0.5 mg/ml, and 1 mg/ml of BSA were 31.82%, 44.72%, and 48.71%, respectively, whereas in MBAuNPs-BSA suspensions with equivalent BSA concentrations, the α -helix contents were 22.13%, 40.32%, and 43.2%, respectively (Fig. 8).

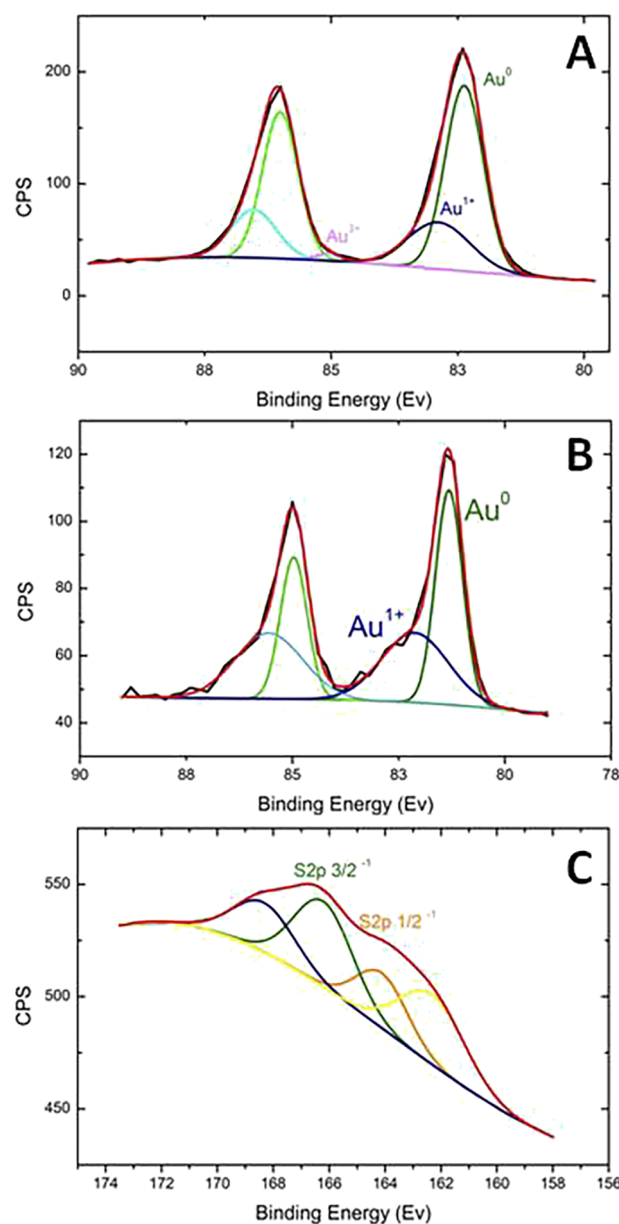


FIG. 7. XPS spectra of MBAuNPs and MBAuNPs-BSA suspensions. High-resolution spectra from Au in MBAuNPs (a) and MBAuNPs-BSA (b) suspensions. (c) High-resolution spectra from sulfur in MBAuNPs-BSA suspensions.

TABLE II. Calculation of the surface area of MBAuNPs containing 8, 12, and 20 peaks, and the number of BSA molecules bound per nanoparticle in the hard and soft corona.

Peaks	Hard corona		Soft corona	
	MBAuNP surface (nm ²)	BSA molecules	MBAuNP surface (nm ²)	BSA molecules
8	24 983	900	52 193	1900
12	30 212	1000	71 000	2500
20	40 668	1500	108 652	3880

TABLE III. Chemical Au and S bonds identified by XPS in MBAuNPs and MBAuNPs-BSA.

Sample	Peak index	Position (eV)	ID
MBAuNPs (Au)	Au ⁰	82.37	Au
	Au ⁰	86.00	Au doublet
	Au ¹⁺	82.87	N–Au (I)
	Au ¹⁺	86.53	Au doublet
	Au ³⁺	85.06	Au (III)
MBAuNPs-BSA (Au)	Au ⁰	81.31	Au
	Au ⁰	84.96	Au doublet
	Au ¹⁺	82.11	C–S–Au (I)
	Au ¹⁺	85.55	Au doublet
MBAuNPs-BSA (S)	S 2p _{3/2}	166.21	S–Au
	S 2p _{1/2}	164.12	S Doublet

BSA and human serum proteins bound to MBAuNPs and MBAuNPs-BSA

After exposing MBAuNPs or MBAuNPs-BSA to human serum for 24 h and washing them by repeated centrifugation with PBS,

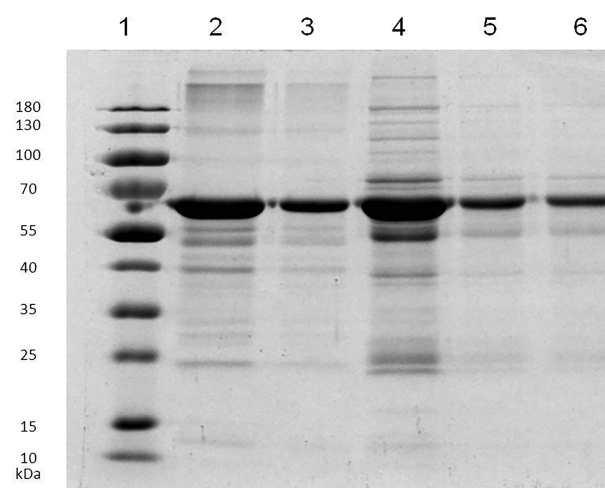


FIG. 9. SDS-polyacrylamide gel electrophoresis of proteins bound to MBAuNPs and MBAuNPs-BSA exposed to human serum. Lane 1, protein molecular markers. Lane 2, BSA in solution (10 µg/µl). Lane 3, pellet from the third wash of MBAuNPs-BSA. Lane 4, human serum. Lane 5, pellet from MBAuNPs exposed to human serum. Lane 6, pellet of MBAuNPs-BSA exposed to human serum.

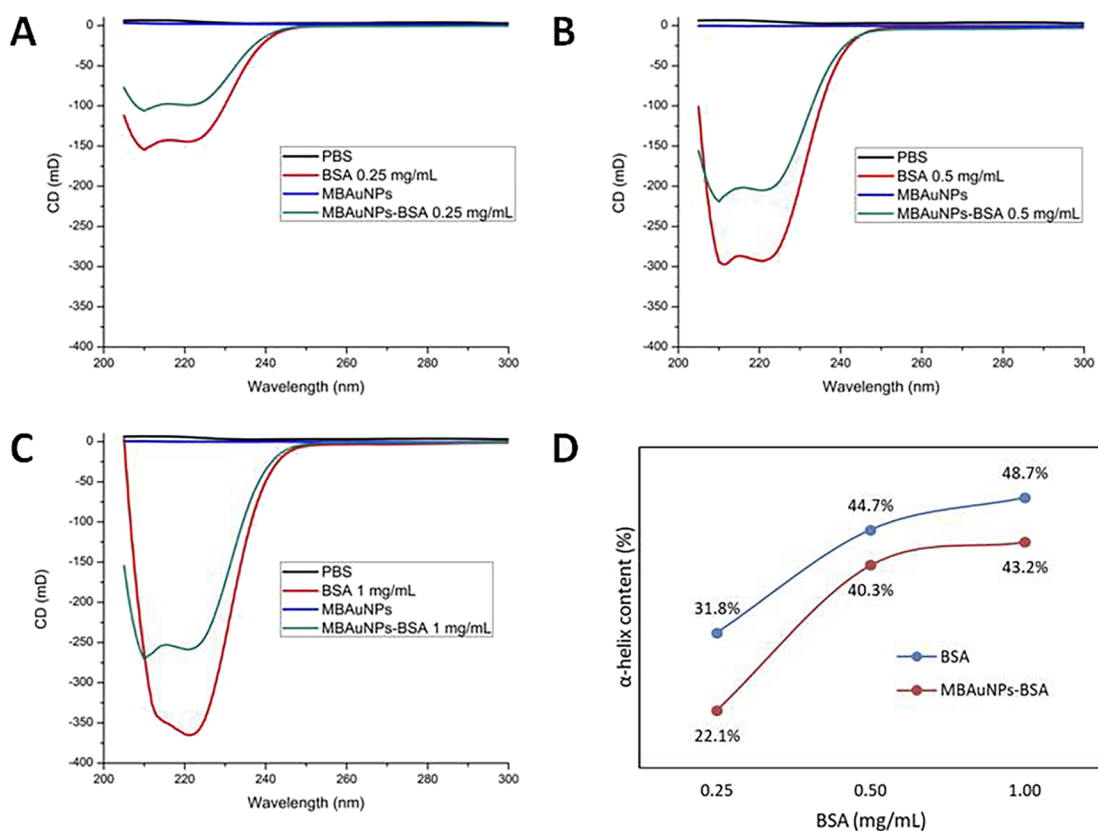


FIG. 8. Circular dichroism spectra and proportion of α -helices from samples with increasing BSA in solutions and MBAuNPs-BSA suspensions. (a) 0.25 mg/ml BSA. (b) 0.5 mg/ml BSA. (c) 1 mg/ml BSA. (d) Proportion of α -helices in BSA solutions and MBAuNPs-BSA suspensions.

the ζ -potential was -18 for MBAuNPs and -31 for MBAuNPs-BSA, PDI was 0.205 for MBAuNPs and 0.167 for MBAuNPs-BSA, and D_H was 148 nm for MBAuNPs and 185 nm for MBAuNPs-BSA.

After having been exposed to human serum, MBAuNPs and MBAuNPs-BSA that were extensively washed by centrifugation and then subjected to denaturing conditions released protein bands with apparent molecular weights of 180 kDa, 156 kDa, 120 kDa, 84 kDa, 75 kDa, and 25 kDa (Fig. 9).

DISCUSSION

The MBAuNPs described in this paper are potentially useful for photothermal ablation of tumors since they induce hyperthermia by irradiation with a near-infrared laser at minimum power both in aqueous suspensions and in phantom gels mimicking the human skin.

The auric seeds, synthesized as precursors of MBAuNPs, are spherical and stable as expected,²⁰ they present maximum absorbance at 520 nm and have excellent stability and dispersion as shown by dynamic light scattering (DLS) analysis. Their concentration was determined by the ICP-MS method of Allabashi *et al.*,²¹ used also to control the amount of seeds used for the synthesis of anisotropic MBAuNPs, that was carried out with a modification of the method of Maiorano *et al.*²² The resulting MBAuNPs had maximum absorbance at 775 nm, indicating an increased efficiency to produce hyperthermia by NIR irradiation, whereas the loss of the 520 nm absorbance peak suggests that each seed gives rise to a single MBAuNP. The larger shift of the absorption peak toward the infrared by our MBAuNPs may be due to the relatively high HEPES concentration (50 mM) used for their synthesis, leading to an increased length of the cones attached to the seed surface.

The highest photothermal efficiency was attained with suspensions containing 3 mg/l of MBAuNPs in phantom gels irradiated with the 808 nm laser at 0.75 W/cm², whose temperature was increased by 4.8 °C, well above the results obtained in previous studies.^{23–26} Our finding that the hyperthermia of phantom gels depends on both the MBAuNP concentration and irradiation power may be further tested in cell cultures and animal models.

Functionalization with specific ligands to direct MBAuNPs to diseased tissues is expected to improve their therapeutic efficacy when administered systemically through intravenous injection. However, such functionalization may be affected and even nullified by the protein corona that instantaneously forms on their surface, even in MBAuNPs previously functionalized with BSA to prevent their agglomeration and to direct them to the albumin receptors that abound on the surface of the endothelial cells forming the inner wall of blood vessels.²⁷

HRTEM images of extensively washed MBAuNPs-BSA have a 10 nm– 15 nm thick halo absent from naked MBAuNPs and resolved individual BSA molecules appearing to form a tapestry of one or two molecular layers. The thickness of the protein layer is consistent with the $8 \times 8 \times 3.5$ nm³ dimensions of the native BSA molecule.²⁸ The 50 nm displacement of the absorbance peak from 775 nm in MBAuNPs to 825 nm in MBAuNPs-BSA is higher than the 7 nm displacement reported by Nghiem *et al.*²⁹ This difference may be due to a difference in the number of BSA molecules bound per nanoparticle since the magnitude of the

displacement depends on the initial BSA concentration used for functionalization.

Our mathematical estimation of the surface area of MBAuNPs and the number of BSA molecules bound to their surface matches the number of BSA molecules determined by UV spectrophotometry. Taking into account the HRTEM images, the increase of the hydrodynamic diameter, the mathematical estimation of the surface area, and the experimental quantification results, it appears that the PC of MBAuNPs-BSA has two parts: an internal film of one or two layers of BSA molecules covalently bound to the MBAuNP surface, and a lax external layer formed by agglomerated BSA molecules linked by non-covalent bonds that are released by extensive washing. This model is consistent with that of Kokkinopoulou *et al.*³⁰ who proposed that the protein corona consists not only of multiple layers covering each NP but also a three-dimensional network of proteins linked to the NP surface.

Brewer *et al.*³¹ estimated that the number of BSA molecules bound to spherical AuNPs ranges from 2.0×10^{12} cm⁻² to 3.3×10^{12} cm⁻² depending on the orientation in which BSA is bound. Assuming that the area of each BSA molecule to be 28 nm² and applying it to auric seeds and MBAuNPs, we obtained a similar range: 3.5×10^{12} BSA molecules per cm².

To calculate the surface area of MBAuNPs, we used Eq. (3) to estimate the area that would bind the hard corona and a slightly modified Eq. (4) for the area available for the soft corona. Our results were similar to the values of the area for MBAuNPs calculated by Tsoulos *et al.*,³² and for the number of molecules attached to a given Au surface published by Brewer *et al.*³¹

NPs with ζ -potential values $\geq +30$ or ≤ -30 are considered stable.³³ Our spheric seeds (ζ -potential = -36.8 mV) are quite stable and do not agglomerate for months, whereas our MBAuNPs (ζ -potential = -24.4 mV) tend to agglomerate. Since our MBAuNPs-BSA have a ζ -potential = -72.7 mV, we confirmed that BSA decreases their tendency to agglomerate³⁴ and turn them into a stable system.

High-resolution XPS analyses allowed us to unambiguously determine the presence of C–S–Au bonds between BSA molecules and gold atoms on the MBAuNP surface,³⁵ they are probably Au–S cystine disulfide coordination bonds as those described by Wang *et al.*³⁶ Each BSA molecule contains 34 cysteine residues and a free thiol at Cys34 that most likely is involved in the covalent binding of BSA to the gold surface, making MBAuNPs-BSA stable.

Assessment of the secondary BSA structure in solution and that bound to MBAuNPs revealed a decrease in the proportion of α -helices on the functionalized protein. Disulfide bonds are the main form of sulfur in BSA that stabilizes α -helices to maintain the protein structure. XPS analysis indicates that BSA binding to the MBAuNP surface through S–Au bonds may decrease the proportion of α -helices. Similar changes in the secondary protein structure have already been reported,^{36,37} and it is not known if these changes affect the affinity of BSA to the receptor-binding domain located on the surface of endothelial cells and some cancer cells.²⁷

We also found that exposure of MBAuNPs and MBAuNPs-BSA to human serum increased their ζ -potential values close to those of uncoated MBAuNPs, and also increased D_H values of 23 nm for MBAuNPs and 39 nm for MBAuNPs-BSA. These effects may be explained by the presence of human serum molecules other

than BSA or HSA and led us to characterize the electrophoretic patterns of the proteins bound to MBAuNPs and MBAuNPs-BSA exposed to human serum. HSA and other unidentified proteins with apparent molecular weights of 180 kDa, 156 kDa, 120 kDa, 84 kDa, 75 kDa, and 25 kDa bound both to MBAuNPs and MBAuNPs-BSA were associated with the higher increase of ζ -potential and D_H in MBAuNPs-BSA, suggesting that previous functionalization with BSA affects the binding of human serum proteins.

This study reinforces the potential of MBAuNPs for photothermal tumor ablation. Their use in medical application, however, depends greatly on the successful delivery to their biological targets through the fine control and tuning of the protein corona, a process that requires research by oncologist/molecular biologist/physicist teams.

Experimental

Materials

Chloroauric acid (HAuCl_4) (USA), Hepes sodium salt (99.5%) (USA), hydroxylamine (NH_2OH) (China), 99% sodium citrate (USA), bovine serum albumin (BSA) (96%) (USA), agar (Portugal), and polyethylene powder (USA) were purchased from Sigma-Aldrich. TX-151 was purchased from Balmar, L.L.C. (USA), Nonidet P40 (ultrapure) from Thermo Scientific (USA), hydrochloric acid (HCl) from J. T. Baker (USA), and nitric acid (HNO_3) from CTR Scientific (USA).

Synthesis of auric seeds

Synthesis of spherical seeds was performed using the Turkevich method in mixtures containing 25 mM HAuCl_4 and 0.75 mM sodium citrate, pH 7.4, as a reducing agent.^{20,38,39} Briefly, 19.8 ml of 0.75 mM sodium citrate pH 7.4 was added to a 30 ml beaker with a magnetic bar, and the mix was stirred on a magnetic hot plate at 70 °C; 0.2 ml of 25 mM HAuCl_4 was immediately added, and the mixture was kept under the same conditions for 10 min until the color was changed from light gray to red, with the appearance of red wine. When the reaction ended, the UV-VIS spectrum was recorded in a Cary model 60 Agilent spectrophotometer. To determine the shape and size of NPs, the samples were also analyzed by dynamic light scattering (DLS) with a zetameter (Zetatract, Microtrac) and with a Dual Beam FEI-Helios Nanolab 600 scanning electron microscope (SEM) from which images were obtained at 5 kV, 88 pA, 4 mm working distance, and 300 000 \times magnification.

MBAuNP synthesis

MBAuNPs were synthesized in mixtures containing 0.8 mM HAuCl_4 , 1×10^{15} auric seeds per l (60 mg/l of Au), 100 mM hydroxylamine (NH_2OH), and 50 mM Hepes pH 7.4. The spectrophotometer probe (A_{300} – A_{1000} , average reading speed) was kept immersed in a 30 ml beaker containing a magnetic bar and placed in a container with ice to keep the mixture at 4 °C, and the absorbance measurements were recorded at the start and every 2 min while the reaction occurred; 12.5 ml of 50 mM Hepes pH 7.4 μl , 150 μl of seed suspension, 400 μl of 100 mM hydroxylamine, and 2.2 ml of 0.8 mM HAuCl_4 (one drop every 8 s) were successively added.

Auric seed and MBAuNP concentration analyses

Gold content in auric seeds and MBAuNPs

To determine the amount of gold present in auric seeds and MBAuNPs, an aliquot from each sample was digested with HCl and HNO_3 in a water bath for 1 h. Inductively coupled plasma atomic emission spectroscopy (ICP-OES) of samples was performed in a Varian, model 730-ES instrument.

Concentration of auric seeds

The Au concentration obtained by ICP-OES was used to determine the number of auric seeds per liter,²¹ dividing the total number of gold atoms in the sample by the number of atoms per NP, with the following formulas:

$$N_{at} = N_A \pi \rho D^3 / 6M, \quad (1)$$

$$N = A_t / N_{at}, \quad (2)$$

where N_{at} = Average number of Au atoms per nanoparticle, N_A (Avogadro's number) = 6.022×10^{23} atoms/mol, ρ (fcc density of the seeds) = 1.93×10^{-20} g/nm³, D (diameter of the nanoparticles) = 18 nm, M (gold atomic weight) = 197 g/mol, and A_t (total number of atoms in the sample) = 1.834×10^{20} atoms/l, obtained from the ICP-OES analysis.

Mathematical approach to estimate the surface area of MBAuNPs

To determine the surface area of MBAuNPs, their shape was modeled as a "piñata," i.e., a structure formed by a spherical core to whose surface are attached the bases of cones with blunt tips. The total surface area of each MBAuNP would be given by the following contributions: (i) the total area of the spherical core, minus (ii) the area of the sphere caps that occupy the N bases of the cones, plus (iii) the area of N cones, plus (iv) N times the area of the half-sphere that forms the tip of the cones.³² The terms appear in the same order in the following equation for the total area:

$$A(1) = 4\pi a^2 - 2\pi a \sum_{i=1}^N \left(a - \sqrt{a^2 - R_i^2} \right) + \sum_{i=1}^N \left\{ \pi(r_i + R_i) \sqrt{(R_i - r_i)^2 + h_i^2} + 2\pi r_i^2 \right\}, \quad (3)$$

where core average radius: $a = 34$ nm, average tip radius: $r_i = 4.67$ nm, average tip length: $h_i = 29.16$ nm, and average radius at the base of the tip: $R_i = 15.1$ nm.

The values assigned to these variables originate from the statistics of the SEM micrographs of our MBAuNPs.

Figure 10 illustrates "piñata-like" NPs with 8 and 20 tips, where N is the number of peaks per NP. Considering that MBAuNPs have different numbers of tips, a first geometric approximation was used with N values of 8, 12, and 20.⁴⁰

Hyperthermia assays with auric seeds or MBAuNPs in aqueous suspensions and phantom gels

These assays were performed with MBAuNP aqueous suspensions in 500- μl microcentrifuge tubes or MBAuNP suspensions

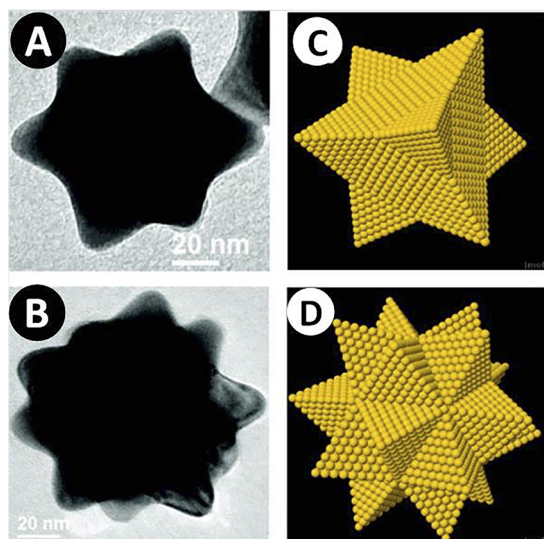


FIG. 10. Images and models of gold nanoparticles with 8 and 20 tips. Transmission electron microscopy images of gold nanoparticles with 8 tips (a) and 20 tips (b). Models simulating the 8 tip-image (c) and the 20 tip-image (d). Reproduced with permission from Cabrera-Trujillo *et al.*, *J. Phys. Chem. C* 114, 21051 (2010). Copyright 2010 American Chemical Society.

in phantom gels, both of which were irradiated for 10 min with an 808 nm laser (Lasermate model IML-808) at different powers (0.45 W/cm², 0.75 W/cm², and 1 W/cm²). The temperature of each sample was measured with an infrared thermal camera (Flexcam R2 model IR) from time zero until the end of the irradiation period. To prepare phantom gels resembling human tissues,⁴¹ we prepared a suspension containing MBAuNPs (2 mg/l or 3 mg/l of Au), 100 ml of ultrapure water, 1.5 g of agar, and 2.5 g of TX-151, all added to a vacuum flask. The mixture was heated in a microwave oven for 15 s periods until complete agar and TX-151 dissolution was reached. To the mixture, kept under stirring at 50 °C, 5 ml of an MBAuNP suspension (containing 2 μg or 3 μg of gold, equivalent to 1.3 × 10¹⁰ or 1.9 × 10¹⁰ MBAuNPs per ml, respectively), 2 g of polyethylene powder was added. After polyethylene dissolution, air bubbles were eliminated by aspiration with a vacuum pump (Welch, Model 2522). The mixtures were poured onto 35 × 10 mm² Petri dishes and left to solidify overnight at room temperature.

Functionalization of MBAuNPs with BSA

For functionalization, MBAuNPs (7.6 × 10¹¹ MBAuNP/ml) were washed five times by centrifugation with 0.1% Nonidet P40 aqueous solution. For the last wash, phosphate-buffered saline (PBS: 137 mM NaCl, 27 mM KCl, 10 mM Na₂HPO₄, 18 mM KH₂PO₄ pH 7.4) was used, and the UV-VIS spectrum was recorded before and after functionalization. After the sixth wash, the supernatant was removed by aspiration, and the pellet was sonicated in an ultrasonic bath (Branson, Model 2800) for 4 min, and vortexed for 15 s; 1 ml of BSA (10 μg/μl) was added, and the mixture was vortexed immediately to prevent MBAuNP agglomeration. The MBAuNPs-BSA suspension was kept at 4 °C for 24 h and then washed

four times by centrifugation with PBS to eliminate the BSA in solution.

BSA quantitation

Calculation using UV-VIS spectra

Since the maximum absorption peak of BSA is at 280 nm (A_{280}), the BSA concentration in solution and MBAuNPs was determined by measuring A_{280} . The molar extinction coefficients of BSA in solution and MBAuNP-BSA suspensions were calculated by comparing the slopes of standard curves of BSA in solution and MBAuNP-BSA suspensions, using a 0.2 cm optical path quartz cell. To determine the average number of BSA molecules per MBAuNP, seven consecutive washes by centrifugation with PBS were carried out after 24 h of exposure to BSA, by dividing the number of MBAuNPs by the number of BSA molecules (estimated from A_{280} and the molar extinction coefficient).

Mathematical estimation of the number of BSA molecules per MBAuNP

The mathematical approximation to calculate the number of BSA molecules per MBAuNP was performed by dividing the total available surface area of the MBAuNP (calculated as explained above) by the area of native BSA molecules. Each native BSA molecule has a tridimensional structure with an area of 28 nm² (Fig. 11).^{28,42}

Assuming a bimolecular BSA layer, the total area of the protein corona on the surface of each MBAuNP-BSA would be

$$A(2) = A(1) + \sum_{i=1}^N \left\{ \pi(r_i + R_i) \sqrt{(R_i - r_i)^2 + h_i^2} + 2\pi r_i^2 \right\}. \quad (4)$$

For a uniform 4-nm-thick protein hard corona, the following values were used: average tip radius: $r_i = 8.67$ nm, average tip length: $h_i = 33.16$ nm, and average radius of the tip base: $R_i = 18.1$ nm. The new total area available will then be divided by the area of native BSA molecules.

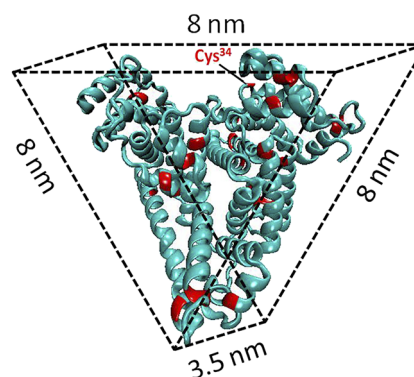


FIG. 11. Diagram of the native BSA tridimensional structure. The image shows the 3D structure of BSA as an equilateral triangular prism. Cysteine 34 may be involved in the binding of BSA to gold. Reproduced with permission from Yu *et al.*, *Nanoscale* 8, 14393 (2016). Copyright 2016 Author(s), licensed under a Creative Commons Attribution 4.0 License.

Characterization of MBAuNPs and MBAuNPs-BSA

Scanning electron microscopy (SEM)

To a 1.5 ml microcentrifuge tube containing 500 μl of ethanol, 1 ml of the MBAuNP reaction mixture was added. The tube was immersed in an ultrasonic bath for 5 min, vortexed for 20 s, and centrifuged for 10 min at 13 000 rpm ($15\,304 \times g$) and 4 °C. The supernatant was removed by careful aspiration, and 1 ml of ultra-pure water was added to the pellet that was further washed by centrifugation six more times. On an aluminum sample holder (pin), 75 μl -samples were deposited and left to dry overnight before observing them in a scanning electron microscope (Dual Beam FEI-Helios Nanolab 600) at 150 000 \times magnification, 5 kV, 88 pA, and 4 mm working distance.

Transmission electron microscopy (TEM, HRTEM)

Pure and functionalized MBAuNP samples were stained with uranyl acetate in Petri dishes covered with Parafilm. On a grid (Lacey Carbon), a drop of a concentrated sample was applied and allowed to sediment for 2 h at room temperature. After adding uranyl acetate (10 $\mu\text{g}/\mu\text{l}$), the samples were left to dry for 15 min and then were observed with a Jeol 200 CX 100 keV transmission electron microscope (TEM) and a Jeol ARM200F high-resolution transmission electron microscope (HRTEM).

X-ray photoelectron spectroscopy (XPS)

One drop of either MBAuNPs or MBAuNPs-BSA suspension was placed on $1 \times 1 \text{ cm}^2$ silicon plates. The plates were left to dry at room temperature for 24 h and analyzed in an ultra-high vacuum with an XPS PHI-5000 spectrometer (Physical Electronics, VersaProbe II Model), and the results were processed with the XPS Multipak software.

Human serum

Human blood obtained with informed consent from healthy donors following the Declaration of Helsinki was left to clot spontaneously. Clotted blood was centrifuged for 10 min at 13 000 rpm, and the supernatant serum was transferred to 15 ml plastic tubes. Pooled serum from four volunteers was stored at $-80 \text{ }^\circ\text{C}$ until it was used.

Dynamic light scattering (DLS)

The ζ -potential and size of MBAuNPs and MBAuNPs-BSA were determined by DLS at 22 °C and 90° dispersion angles with a zetameter (Zetatrac, Microtrac). 0.1% Nonidet P40, PBS, BSA dissolved in PBS, and human serum were used as vehicles to prepare MBAuNPs and MBAuNPs-BSA suspensions.

Sodium dodecyl sulfate-polyacrylamide gel electrophoresis

The interaction of MBAuNPs with BSA and with human serum was assessed using sodium dodecyl sulfate (SDS)-polyacrylamide gel electrophoresis (SDS-PAGE) of suspension samples washed three times by centrifugation after a 24 h exposure at 37 °C. 10- μl from each sample was mixed with 10 μl of Laemmli buffer (10% 2-mercaptoethanol, 0.004% Bromphenol blue, 20% glycerol, 4% sodium dodecyl sulfate, 125 mM Tris-HCl, pH 6.8), and the mixtures were boiled for 5 min at 100 °C. 20- μl volumes were applied

to 12% polyacrylamide slab gels, run for 2 h at 120 V, stained with Coomassie Blue for 30 min, and destained overnight in a 5:4:1 methanol-water-glacial acetic acid mixture.

Circular dichroism (CD)

To determine the proportion of α -helices from BSA both in solution and bound to MBAuNPs, circular dichroism (CD) measurements were performed at 4 °C in a 0.2 cm quartz cell with a 205 nm–330 nm reading range in a MOS-500 spectropolarimeter (BioLogic Science Instruments). In mixtures with a 7.6×10^{11} MBAuNPs/ml fixed concentration dissolved in PBS, the BSA concentrations tested were 1.0 mg/ml, 0.5 mg/ml, and 0.25 mg/ml. The proportion of α -helices from BSA in solution or bound to MBAuNPs was calculated with the following formulas:^{43,44}

$$MRE = \text{Observed DC (mdeg)} / 10C_pnl, \quad (5)$$

$$\alpha - \text{Helix}(\%) = (MRE_{222} - 4000 / 33\,000 - 4000) \times 100, \quad (6)$$

where *MRE* = mean residual ellipticity, *Observed DC* (mdeg) = ellipticity obtained directly from DC, *C_p* = molarity of the protein, *n* = number of amino acid residues in BSA, and *l* = path length of the cell in centimeters.

The 4000 and 33 000 values denote the total ellipticity values of the β -sheet form and the pure α -helix form of the protein at 208 nm and 222 nm.

CONCLUSIONS

From spherical Au seeds ($D_H = 18 \text{ nm}$, surface = 1020 nm², A_{max} at 520 nm, ζ -potential = -36.8 mV , and PDI = 0.602), piñata-like MBAuNPs (8–20 peaks, $D_H = 125 \text{ nm}$, A_{max} at 775 nm, ζ -potential = -24.4 mV , and PDI = 0.455) are stoichiometrically synthesized. The surface area of MBAuNPs ranges from 24 984 nm² to 40 669 nm². MBAuNPs are potentially useful for photothermal tumor ablation since they induce hyperthermia of more than 4 °C in phantom gels irradiated with an 808 nm laser source with a power of 0.75 W/cm². MBAuNPs exposed to BSA acquire a protein corona with an internal “hard” portion composed by one or two layers of BSA molecules covalently bound to the surface of each nanoparticle (1500 molecules per MBAuNP), and an external “soft” portion formed by non-covalent bound agglomerated BSA molecules. BSA functionalization decreases the tendency of MBAuNPs to aggregate but increases the polydispersity index, indicative of greater size dispersion. MBAuNPs and MBAuNPs-BSA exposed to human serum bind HSA and other human serum proteins ranging from 25 kDa to 180 kDa, which decrease their stability and increase their D_H , especially in MBAuNPs-BSA.

ACKNOWLEDGMENTS

We are grateful to IPICYT and the National Nanosciences and Nanotechnology Research Laboratory (LINAN) for allowing us to use their facilities, and especially to Dr. Gladis J. Labrada-Delgado and Dr. Mariela Bravo for their support on SEM and XPS analyses, Dr. Araceli Patrón (DBM-IPICYT) for her support on TEM characterization, Dr. Daniel Bahena (IPN) for his support on HRTEM characterization, M.Sc. Dulce Partida Gutiérrez for her support on

DLS characterization, and Q.F.B. Felipe de Jesús Herrera Ponce for his help with XPS data analysis. We also acknowledge Biol. Mireya Sánchez-Garza and Dr. Angélica Montoya Contreras for their excellent technical and administrative support. Finally, we thank Professor Francisco Javier González (CIACYT-UASLP) who supplied the thermal camera for the hyperthermia assays. We thank CONACyT for the Apoyo a la Infraestructura 2016 Grant Nos. 269102 and Problemas Nacionales 216315, and for the scholarship (Grant No. 333131) granted to CCA.

The authors declare no competing financial interest.

REFERENCES

- ¹J. Beik, Z. Abed, F. S. Ghoreishi, S. Hosseini-Nami, S. Mehrzadi, A. Shakeri-Zadeh, and S. K. Kamrava, *J. Controlled Release* **235**, 205 (2016).
- ²Z. Dai, *Advances in Nanotheranostics I* (Springer Berlin Heidelberg, Berlin, Heidelberg, 2016).
- ³S. Gao, M. Zheng, X. Ren, Y. Tang, and X. Liang, *Oncotarget* **7**, 57367 (2016).
- ⁴S. Toraya-Brown and S. Fiering, *Int. J. Hyperthermia* **30**, 531 (2014).
- ⁵R. Weissleder, *Nat. Biotechnol.* **19**, 316 (2001).
- ⁶S. Cho, M. H. Shin, Y. K. Kim, J.-E. Seo, Y. M. Lee, C.-H. Park, and J. H. Chung, *J. Invest. Dermatol. Symp. Proc.* **14**, 15 (2009).
- ⁷S. M. Schieke, P. Schroeder, and J. Krutmann, *Photodermatol., Photoimmunol., Photomed.* **19**, 228 (2003).
- ⁸T. Curry, R. Kopelman, M. Shilo, and R. Popovtzer, *Contrast Media Mol. Imaging* **9**, 53 (2014).
- ⁹P. R. Sajanlal, T. S. Sreeprasad, A. K. Samal, and T. Pradeep, *Nano Rev.* **2**, 5883 (2011).
- ¹⁰Z. Y. Ong, S. Chen, E. Nabavi, A. Regoutz, D. J. Payne, D. S. Elson, D. T. Dexter, I. E. Dunlop, and A. E. Porter, *ACS Appl. Mater. Interfaces* **9**, 39259 (2017).
- ¹¹R. García-Álvarez, M. Hadjidemetriou, A. Sánchez-Iglesias, L. M. Liz-Marzán, and K. Kostarelos, *Nanoscale* **10**, 1256 (2018).
- ¹²B. Van de Broek, N. Devoogdt, A. D'Hollander, H.-L. Gijs, K. Jans, L. Lagae, S. Muyltermans, G. Maes, and G. Borghs, *ACS Nano* **5**, 4319 (2011).
- ¹³C. Corbo, R. Molinaro, A. Parodi, N. E. Toledano Furman, F. Salvatore, and E. Tasciotti, *Nanomedicine* **11**, 81 (2016).
- ¹⁴F. Pederzoli, G. Tosi, M. A. Vandelli, D. Belletti, F. Forni, and B. Ruozi, *Wiley Interdiscip. Rev.: Nanomed. Nanobiotechnol.* **9**, e1467 (2017).
- ¹⁵V. H. Nguyen and B.-J. Lee, *Int. J. Nanomed.* **12**, 3137 (2017).
- ¹⁶P. Foroozandeh and A. A. Aziz, *Nanoscale Res. Lett.* **10**, 221 (2015).
- ¹⁷C. Corbo, R. Molinaro, M. Tabatabaei, O. C. Farokhzad, and M. Mahmoudi, *Biomater. Sci.* **5**, 378 (2017).
- ¹⁸D. Khang, Y. K. Lee, E.-J. Choi, T. J. Webster, and S.-H. Kim, *Int. J. Nanomed.* **10**, 97 (2014).
- ¹⁹L. Treuel, D. Docter, M. Maskos, and R. H. Stauber, *Beilstein J. Nanotechnol.* **6**, 857 (2015).
- ²⁰J. Kimling, M. Maier, B. Okenve, V. Kotaidis, H. Ballot, and A. Plech, *J. Phys. Chem. B* **110**, 15700 (2006).
- ²¹R. Allabashi, W. Stach, A. de la Escosura-Muñiz, L. Liste-Calleja, and A. Merkoçi, *J. Nanopart. Res.* **11**, 2003 (2009).
- ²²G. Maiorano, L. Rizzello, M. A. Malvindi, S. S. Shankar, L. Martiradonna, A. Falqui, R. Cingolani, and P. P. Pompa, *Nanoscale* **3**, 2227 (2011).
- ²³C. J. Gannon, C. Patra, R. Bhattacharya, P. Mukherjee, and S. A. Curley, *J. Nanobiotechnol.* **6**, 2 (2008).
- ²⁴S. Munireddy, S. Katz, P. Somasundar, and N. J. Espot, *J. Gastrointest. Oncol.* **3**, 69 (2012).
- ²⁵Y. Li, R. E. Brown, and R. C. G. Martin, *J. Surg. Res.* **181**, 250 (2013).
- ²⁶L. Mocan, C. Matea, F. A. Tabaran, O. Mosteanu, T. Pop, C. Puia, L. Agoston-Coldea, G. Zaharie, T. Mocan, A. D. Buzoianu, and C. Iancu, *Biomaterials* **119**, 33 (2017).
- ²⁷A. M. Merlot, D. S. Kalinowski, and D. R. Richardson, *Front. Physiol.* **5**, 299 (2014).
- ²⁸X. M. He and D. C. Carter, *Nature* **358**, 209 (1992).
- ²⁹T. H. L. Nghiem, T. H. La, X. H. Vu, V. H. Chu, T. H. Nguyen, Q. H. Le, E. Fort, Q. H. Do, and H. N. Tran, *Adv. Nat. Sci.: Nanosci. Nanotechnol.* **1**, 025009 (2010).
- ³⁰M. Kokkinopoulou, J. Simon, K. Landfester, V. Mailänder, and I. Lieberwirth, *Nanoscale* **9**, 8858 (2017).
- ³¹S. H. Brewer, W. R. Glomm, M. C. Johnson, M. K. Knag, and S. Franzen, *Langmuir* **21**, 9303 (2005).
- ³²T. V. Tsoulos, L. Han, J. Weir, H. L. Xin, and L. Fabris, *Nanoscale* **9**, 3766 (2017).
- ³³A. S. Dukhin and R. Xu, *Charact. Nanoparticles* (Elsevier, 2020), pp. 213–224.
- ³⁴S. Bhattacharjee, *J. Controlled Release* **235**, 337 (2016).
- ³⁵P. Wu, P. Bai, Z. Lei, K. P. Loh, and X. S. Zhao, *Microporous Mesoporous Mater.* **141**, 222 (2011).
- ³⁶L. Wang, J. Li, J. Pan, X. Jiang, Y. Ji, Y. Li, Y. Qu, Y. Zhao, X. Wu, and C. Chen, *J. Am. Chem. Soc.* **135**, 17359 (2013).
- ³⁷P. Wang, X. Wang, L. Wang, X. Hou, W. Liu, and C. Chen, *Sci. Technol. Adv. Mater.* **16**, 034610 (2015).
- ³⁸G. Frens, *Nat. Phys. Sci.* **241**, 20 (1973).
- ³⁹J. Turkevich, P. C. Stevenson, and J. Hillier, *Discuss. Faraday Soc.* **11**, 55 (1951).
- ⁴⁰J. M. Cabrera-Trujillo, J. M. Montejano-Carrizales, J. L. Rodríguez-López, W. Zhang, J. J. Velázquez-Salazar, and M. José-Yacamán, *J. Phys. Chem. C* **114**, 21051 (2010).
- ⁴¹N. Chahat, M. Zhadobov, S. Alekseev, and R. Sauleau, *Electron. Lett.* **48**, 67 (2012).
- ⁴²S. Yu, A. Perálvarez-Marín, C. Minelli, J. Faraudo, A. Roig, and A. Laromaine, *Nanoscale* **8**, 14393 (2016).
- ⁴³A. Selva Sharma and M. Ilanchelian, *J. Phys. Chem. B* **119**, 9461 (2015).
- ⁴⁴Y. Yu, Z. Luo, C. S. Teo, Y. N. Tan, and J. Xie, *Chem. Commun.* **49**, 9740 (2013).